IEEE Access
Multidisciplinary ⋮ Rapid Review ⋮ Open Access Journal

Received 7 August 2024, accepted 20 August 2024, date of publication 26 August 2024, date of current version 4 September 2024.

Digital Object Identifier 10.1109/ACCESS.2024.3449812

RESEARCH ARTICLE

Deep Learning-Assisted Signal Detection for OTFS-NOMA Systems

INCI UMAKOGLU[1], (Member, IEEE), MUSTAFA NAMDAR[1], (Member, IEEE), AND ARIF BASGUMUS[2], (Member, IEEE)

[1]Department of Electrical and Electronics Engineering, Kutahya Dumlupinar University, 43100 Kütahya, Türkiye
[2]Department of Electrical and Electronics Engineering, Bursa Uludag University, 16059 Bursa, Türkiye

Corresponding author: Inci Umakoglu (inci.umakoglu@dpu.edu.tr)

ABSTRACT Orthogonal time frequency space (OTFS) modulation is introduced as a modulation technique known for its strong performance in high-Doppler scenarios. This two-dimensional modulation method involves multiplexing information symbols in the delay-Doppler (DD) domain. This study presents a deep learning (DL) based signal detection for OTFS non-orthogonal multiple access (NOMA) communication networks. In this work, the OTFS known as a popular sixth-generation (6G) candidate solution with enhanced spectral efficiency in high-mobility environments, is combined with NOMA over Rayleigh fading channels. In addition, a DL-based signal detection approach for the OTFS-NOMA scheme is proposed, where the network is trained to distinguish and decode the signals effectively. This enhances the overall system performance and paves the way for more efficient and reliable communication in high-mobility wireless environments. In our study, signal recovery employs a bidirectional long short-term memory (BiLSTM) network. The comparison of the message passing (MP) algorithm and the BiLSTM technique regarding symbol error rate (SER) performance for detecting signals over near and far users is evaluated. Furthermore, we examine the impact of the three common optimizers on the SER achievement for training optimizer selection. Moreover, the numerical results show that the root mean squared propagation (RMSprop) outperforms the other optimizer selection techniques regarding SER. Finally, the performance of the BiLSTM technique is observed to be better than that of the MP, except for the stochastic gradient descent (SGD) optimizer. RMSprop and the adaptive momentum optimizer (Adam) yield a maximum training accuracy of 99.9%.

INDEX TERMS BiLSTM, deep neural networks, delay-Doppler domain, OTFS-NOMA, RMSprop optimizer.

I. INTRODUCTION

The sixth-generation (6G) wireless network is required to support high-quality wireless communication service for high-mobility environments, such as unmanned aerial vehicle (UAV) communications, high-speed railways, and vehicle-to-vehicle communications [1]. Orthogonal frequency division multiplexing (OFDM) is an important waveform utilized in broadband wireless communication systems similarly, digital subscriber line (DSL), fourth-generation (4G) long-term evaluation (LTE), and fifth-generation (5G) networks. Nonetheless, because the orthogonality of OFDM is disrupted, intercarrier interference (ICI) occurs in such environments due to high Doppler. Although the subcarrier bandwidth of OFDM is flexible in the 5G, it is still limited due to several other constraints to adjust to the conditions of the wireless communication channels [2], [3], [4].

In order to solve the limitation of OFDM, a solution acknowledged orthogonal time frequency space (OTFS) has been developed in recent years. A systematic analysis of the considerable performance advantages of OTFS over OFDM was carried out in the literature [5]. The new concept converts time-varying channels into equivalent time-invariant sparse expressions. OTFS sends data symbols in the delay-Doppler

The associate editor coordinating the review of this manuscript and approving it for publication was Frederico Guimarães.

TABLE 1. Summary of the existing literature related to signal detection.

Publication	Summary	A	B	C	D	E
[15], [16]	A survey of zero forcing (ZF) algorithm and linear minimum mean squared error (LMMSE) for OTFS	✓	✓	✓	x	x
[5]	A survey of message passing (MP) algorithm for OTFS	✓	✓	✓	x	x
[17]	A survey of Monte Carlo algorithm for OTFS	✓	✓	✓	x	x
[18], [19]	An overview of machine learning technologies for 6G systems	✓	x	✓	✓	✓
[20]	A review of deep learning aided signal detection for 6G wireless networks	✓	✓	✓	✓	✓
[21]	A survey of channel estimation and signal detection with fully connected deep neural network (FC-DNN) in OFDM systems	✓	✓	✓	✓	✓
[22]	A survey LSTM-based signal detection method for OFDM	✓	x	✓	✓	x
[23]	A survey of signal detection in OFDM systems using RNN with BiLSTM	✓	✓	✓	✓	✓
[24]	A survey of deep learning-based flexible joint channel estimation and signal detection for OFDM-NOMA	✓	✓	✓	✓	x
[25]	A survey of deep learning-based CNN with the scip connections for signal detection in underwater acoustic (UWA) OTFS communication	✓	✓	✓	✓	x

A: Fundamental Limits B: Channel Estimation C: Signal Detection D:Deep Learning Algorithm E:Application Scenarios

(DD) domain while OFDM utilizes the time-frequency (TF) domain. It is known that the DD domain may generate sparse portrayals over time-varying channels, resulting in a considerable improvement in bit error rate (BER) success in the OTFS approach. The sparsity can also be adjusted to refine signal detection and channel estimation [6], [7], [8].

The multiple access mechanism used in an OTFS system with multiple users is an important aspect. The approaches proposed in the literature are classified as orthogonal and non-orthogonal multiple access (OMA and NOMA) techniques [9], [10]. Users are multiplexed in the DD domain in OTFS-OMA and just a single user is allowed to use one particular resource block at a time. Owing to the Doppler spread, the users experienced multi-user interference (MUI) which can be minimized by guard-bands addition. However, this situation has a negative effect on spectral efficiency (SE) [11]. OTFS-NOMA is an alternative method that allows users to share the same source block, and to multiplex in the code or the power domain [12]. NOMA is a well-known approach that can provide better SE than OMA and is recognized as a potential procedure for improving spectrum utilization and user connectivity. In recent years, a variety of OTFS-NOMA methods that use either code domain [13] or power-domain [14] have been recommended in the literature. Power-domain NOMA approaches which employ successive interference cancellation (SIC) and superposition coding (SC) are proven to reach Gaussian broadcast channel capacity.

Improving the efficiency of the OTFS-NOMA network relies significantly on channel equalization and signal detection. Signal detection depends on distinguishing the transmitted symbols from noise and interference. Effective signal detection helps in correctly identifying and decoding the transmitted information. In general, signal detection techniques are classified into linear and nonlinear detection methods. In practical applications, linear signal detection algorithms similarly, the linear minimum mean squared error (LMMSE) and zero-forcing (ZF) are characterized by a notable level of complexity [15], [16]. The Markov chain Monte Carlo [17] and message passing (MP) [5] algorithms are Bayesian-based nonlinear algorithms based on the assumption that they are subject to Gaussian distributed noise. The complexity of nonlinear algorithms is significantly higher compared to the complexity of the LMMSE algorithm, even though these methods can approach optimal performance with many iterations.

With the introduction of new concepts, the demand for much more complicated procedures expanded significantly, and these demands do not appear to be achievable depending on theoretical considerations [18]. Machine learning techniques have tremendous potential to overcome advanced challenges and enhance signal detection performance in wireless communication [19]. While the sample size is large, deep learning (DL) based algorithms are qualified to address the issues effectively [20]. Recently, DL-based approaches have been recognized for their value in communication networks. DL-based solutions can be applied to communication-related problems, including resource allocation, channel estimation, and signal detection. Researchers studied the receiver's channel equalization and demodulation approach with a fully connected deep neural network (FC-DNN) in the OFDM system [21]. The study reveals that the DNN-based receiver is more dependable than the traditional approaches. [22] suggested a long short-term memory (LSTM) based signal detection method. In [23], the authors used a bidirectional long short-term memory (BiLSTM) scheme with the recurrent neural network (RNN) to detect signals. After training, the numerical results indicate that the model accurately traces the channels' features and effectively recovers signals with accuracy and robustness. Reference [24] offers a hybrid channel estimation and signal detection method based on DL in the OFDM-NOMA network. By utilizing a semi-blind joint method for signal detection and channel estimation, they demonstrate that the proposed DL-based detector (DLD) shows advantageous BER success in multi-user OFDM-NOMA scenarios. In [25],

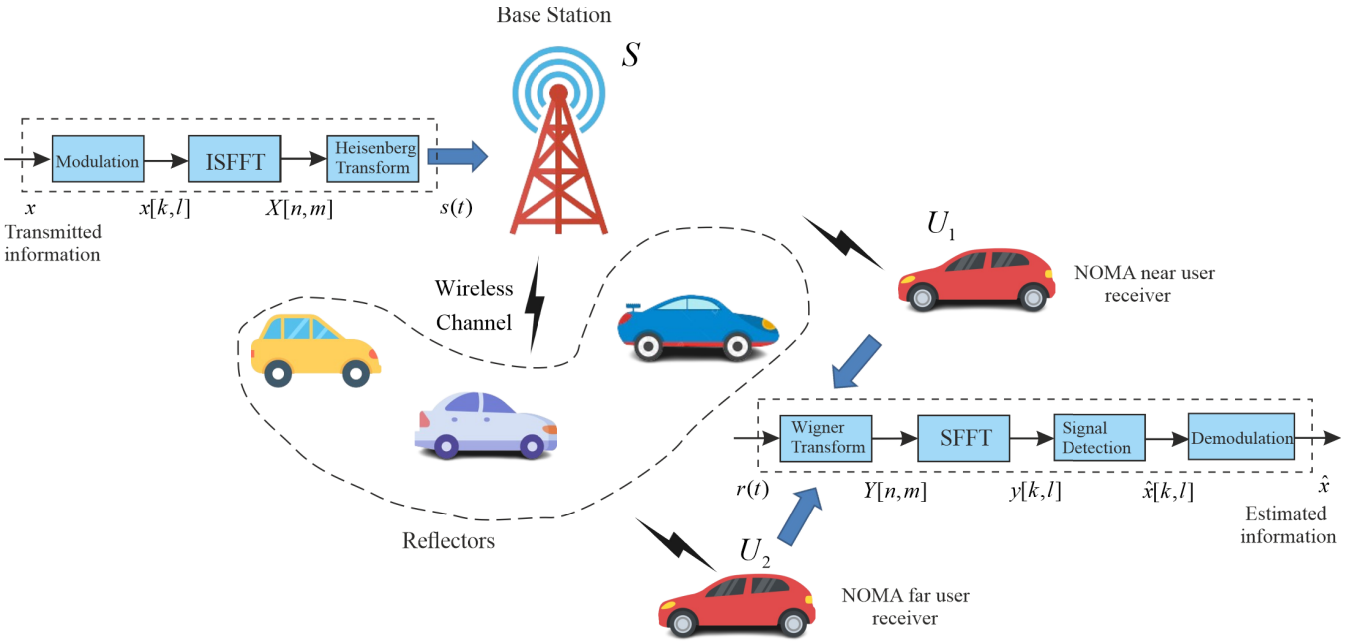

FIGURE 1. OTFS general modulation/demodulation block diagram.

the CNN with the skip connections BiLSTM technique are introduced as a DL-aided neural network for signal detection in underwater acoustic (UWA) OTFS communication. The suggested method outperformed the FC-DNN, MP, and 2D-CNN signal detection algorithms in the UWA-OTFS in terms of BER performance. [26] introduces a signal modulation type recognition approach that utilizes feature fusion and the ResCNN model, specifically designed for scenarios involving fractal noise. In [27], the authors present a novel target recognition method for carrier-free ultra-wide-band radar where the experimental results demonstrate that this approach significantly outperforms existing methods, including CNN. The summary of existing surveys related to signal detection for 5G and beyond applications is presented in Table 1.

II. MAIN CONTRIBUTIONS

As far as observed in the literature, it can be said that there are not many publications on the achievement improvements for the multi-user OTFS-NOMA network. Based on the previous considerations, the objective of the paper is to improve the symbol error rate (SER) of multi-user OTFS-NOMA systems through a DL-based technique. The key contributions of this work are summarized as follows.

- First, the power-domain downlink OTFS-NOMA systems' error rate performances have not been extensively studied. Therefore, we investigate the OTFS-NOMA network for high-mobility users in our article covering channel model and system architecture with delay-Doppler impact. We present a signal detection method based on DL for two users downlink OTFS-NOMA over Rayleigh fading channels.
- Next, in our study MP algorithm and BiLSTM DL-based method have been broadly inspected regarding NOMA users' SER results for signal detection. To the best of our knowledge, this study is one of the very few publications that proposed in DL-based signal detector for the OTFS-NOMA network in the literature.
- Then, when the signal recovery is carried out using a BiLSTM network, we evaluate the SER of three common optimizers for training optimizer selection: the stochastic gradient descent (SGD) optimizer, the adaptive momentum (Adam) optimizer, and the root mean square propagation (RMSprop) optimizer.
- Furthermore, extensive data has been generated by providing the training accuracy and training loss in detail.

The structure of the paper is formed as follows. In Section III, the proposed OTFS-NOMA system model is submitted. In Section IV, the MP algorithm and BiLSTM are outlined for OTFS-NOMA signal detection. In Section V, numerical outcomes are provided to assess the effectiveness of the suggested DLD in downlink OTFS-NOMA. In Section VI, discussions are presented and the study is concluded. Finally, in the last part of the manuscript, a list of abbreviations and acronyms used throughout the paper is given after the VI. Conclusion Section.

III. OTFS-NOMA SYSTEM MODEL

In the OTFS-aided power domain NOMA system framework, high-speed mobile users utilize dissimilar transmission

power while employing the equivalent DD domain source. Figure 1 characterizes an OTFS-assisted downlink NOMA structure including a base station S, three reflectors, and two destination users $K = 2$, namely near and far, $U_i, i \in \{1, 2\}$, respectively [28]. The signal, the target users get is a consolidation of postponed, degraded, and Doppler-shifted copies. The delay is relative to the dimension of each propagation line. In contrast, the Doppler shift is caused by the corresponding act of the receiver and reflectors in the scenario where the transmitter is treated immobile.

A. TF DOMAIN AND DD DOMAIN

TF and DD domains are efficiently employed by OTFS-NOMA [5], [29]. A discrete TF domain is obtained using the period T for sampling and frequency interval f as shown,

$$\Lambda_{TF} = \{(nT, m\Delta f), n = 0, \cdots, N-1, m = 0, \cdots, M-1\}, \tag{1}$$

where $N, M > 0$. As a result, the discrete DD domain is given as

$$\Lambda_{DD} = \{ (k/NT, l/M\Delta f), \\ k = 0, \cdots, N-1, l = 0, \cdots, M-1\}, \tag{2}$$

where N and M indicate the total number of time intervals and frequency subcarriers, respectively.

B. CHANNEL MODEL

Under the presumption of a multi-user wireless communication system with K users, τ delay, and v doppler shift, $h_i(\tau, v)$ is the channel response for $1 \leq i \leq K$ in the DD domain. Mobile channel sparsity in the DD domain is handled to clarify channel estimation and signal perception in OTFS. It is assumed that the propagation lines between the sender and the end user are limited in this case. In the DD domain, the channel impulse response is defined as

$$h_i(\tau, v) = \sum_{p=1}^{P_i} h_{i,p}\delta\left(\tau - \tau_{i,p}\right)\delta\left(v - v_{i,p}\right). \tag{3}$$

The parameters P_i and $\tau_{i,p}$ stand for the number of propagation lines between the sender and user i, respectively. The Doppler shift in the propagation line is characterized by $v_{i,p}$, and the Dirac delta function is defined by δ. The independent and identically distributed (i.i.d) complex Gaussian channel gain is symbolized by $h_{i,p} \sim \mathcal{CN}(0, 1/P_i)$. It is possible to determine the OTFS resolution of Doppler and delay as $1/(M\Delta f)$ and $1/(NT)$, respectively. We consider M and N to be adequately large enough to disregard the impact of delay and Doppler shift. Therefore, the indices corresponding to discrete delay and Doppler shift taps are as follows

$$\tau_{i,p} = l_{i,p}/(M\Delta f), v_{i,p} = k_{i,p}/(NT). \tag{4}$$

C. GENERAL PRINCIPLES OF OTFS

In Figure 1, the OTFS general modulation/demodulation block diagram is presented. $x[k, l]$ is indicated as the information bits which are transmitted as $M \times N$ quadrature amplitude modulation (QAM) symbols. The DD domain signal $x[k, l]$ is then converted into the TF domain signal $X[n, m]$ through the inverse symplectic fast Fourier transform (ISFFT). The $s(t)$ signal is acquired and sent to the communication channel after the Heisenberg transformation is applied to the $X[n, m]$ matrix. The Wigner transform is first utilized on the time domain signal $r(t)$ at the receiver to generate the TF domain signal $Y[n, m]$. A symplectic fast Fourier transform (SFFT) is implemented in the demodulation section to acquire the DD domain signal $y[k, l]$. Ultimately, the signal disclosure technique is employed to detect the signals [5].

The OTFS transmitter sends the symbols of $x_i[k, l]$ in the DD domain, which may be defined with the $X_i[n, m]$ signal in the TF domain as

$$X_i[n, m] = \frac{1}{\sqrt{NM}} \sum_{k=0}^{N-1} \sum_{l=0}^{M-1} x_i[k, l] e^{j2\pi\left(\frac{nk}{N} - \frac{ml}{M}\right)}, \tag{5}$$

where $x_i[k, l]$ indicates the matrix for the i-th user. The Heisenberg transform is then applied to the TF signal matrix $X_i[n, m]$ to generate a continuous-time signal. The signal of the i-th NOMA user is defined

$$s_i(t) = \sum_{n=0}^{N-1} \sum_{m=0}^{M-1} \sqrt{\xi_i \alpha_i} X_i[n, m] g_{tx}(t - nT) e^{j2\pi m\Delta f(t-nT)}, \tag{6}$$

where ξ_i is the transmission power of i-th user, $T = 1/\Delta f$ is the symbol duration and $g_{tx}(t)$ is the pulse shaping waveform for transmission [29]. Here, α_i defines the power allocation (PA) coefficient and $\sum_{i=0}^{K} \alpha_i = 1$. Owing to the necessity for quality of service, the far user is given high priority, $\alpha_2 > \alpha_1$. The signal $s_i(t)$ is sent over a channel, yielding the following expression

$$r_i(t) = \int\int h_i(\tau, v) s_i(t - \tau) e^{j2\pi v(t-\tau)} d\tau dv + w_i(t). \tag{7}$$

Here $w_i(t)$ denotes the complex additive white Gaussian noise (AWGN) term and σ_i^2 is the variance. For the i-th user, the discrete-time signal is $r_i = H_i s + w_i$, where w_i is the $MN \times 1$ complex AWGN vector and H_i is the $MN \times MN$ channel matrix of the i-th user, formed from the impulse responses. The below cross-ambiguity function is computed in a matched filter at the receiver, as defined in the following equation,

$$Y_i(t, f) = \int g_{rx}^*\left(t' - t\right) r_i\left(t'\right) e^{-j2\pi f(t'-t)} dt', \tag{8}$$

where $g_{rx}^*(t)$ indicates the received waveform. By sampling $Y(t, f)$ for the i-th user, the matched filter's output can be given as

$$Y_i[n, m] = Y_i(t, f)|_{t=nT,\, f=m\Delta f}. \tag{9}$$

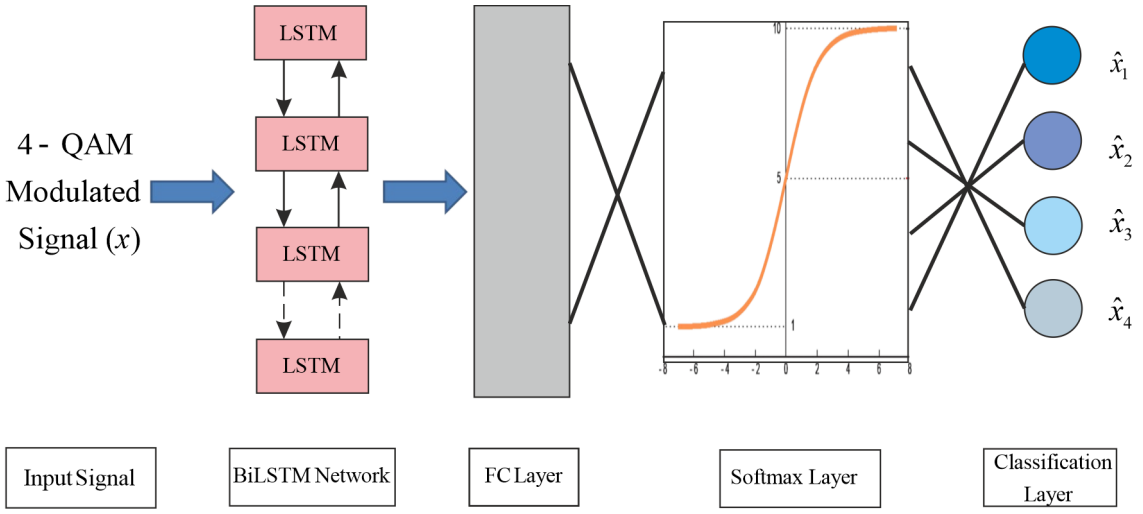

FIGURE 2. Deep learning-aided OTFS-NOMA communication.

The Wigner transformation is represented by the above expressions, (8) and (9). Following that, SFFT is accomplished on $Y_i[n, m]$ samples, and the symbols $y_i[k, l]$ are derived in the DD domain as

$$y_i[k, l] = \frac{1}{\sqrt{NM}} \sum_{n=0}^{N-1} \sum_{m=0}^{M-1} Y_i[n, m] e^{-j2\pi \left(\frac{nk}{N} - \frac{ml}{M}\right)}. \quad (10)$$

The received signal can be designed as follows, assuming that the sent and received pulses are perfectly orthogonal.

$$Y_i[n, m] = H_i[n, m]X_i[n, m] + W_i[n, m], \quad (11)$$

where $W_i[n, m]$ indicates AWGN in the TF domain. Here, $H_i(n, m) = \iint h_i(\tau, v) e^{j2\pi vnT} e^{-j2\pi(v+m\Delta f)\tau} d\tau dv$. Finally, the sent signal can be retrieved as $\hat{x}[k, l]$ through signal detection and demodulation.

IV. BiLSTM-BASED SIGNAL DETECTION FOR OTFS-NOMA

In this study, we investigated two different approaches for signal detection in the OTFS-NOMA network, namely the MP algorithm and BiLSTM. First of all, similar to the study mentioned in [5], we examine the MP algorithm for OTFS-NOMA, which experienced testing within the context of OTFS. In the MP algorithm, the messages conveyed from observation nodes to variable nodes consist of the mean and variance of the interference terms. Conversely, the information transmitted from a variable node to the observation nodes comprises the probability mass function (pmf). A comprehensive explanation of the MP algorithm is provided in [5].

The suggested DL-aided OTFS-NOMA communication model is shown in Figure 2. Here, the DL network is designed to perform signal detection, and this component is replaced by BiLSTM. In the detection component, we presume that the channel impulse response (CIR) is known. The suggested DL network comprises five layers: an input layer, a BiLSTM layer, followed by an FC layer, then a softmax layer and a classification layer at the end. $\hat{x}_1, \hat{x}_2, \hat{x}_3, \hat{x}_4$ symbols for near and far users are estimated as seen in Figure 2. The operations within each layer are outlined as follows:

- The DL network operates using real numbers rather than complex numbers. Hence, the input layer receives both the in-phase (I) and quadrature (Q) components of the received data. Subsequently, the input layer's signal is then conveyed to the LSTM layer.
- The LSTM layer is composed of 600 hidden cells. The selection of the LSTM layer in this paper is based on its capability to learn long-term relationships among time steps in sequence and time series data.
- The signal from the LSTM layer is multiplied by a weight matrix in the FC layer.
- In addition to the aforementioned three layers, two layers are handled: a classification layer and a softmax layer.

Algorithm 1 shows the proposed signal detection of the OTFS-NOMA scheme and outlines the process of generating the dataset for training.

The BiLSTM layer of the neural network comprises two LSTM networks, LSTM-F and LSTM-B, that present in opposite directions, as seen in Figure 3. The inputs are routed into LSTM-F in a forward direction and LSTM-B in a reverse direction. From the beginning to time t, the forward layer does the computation. For each time step, the forward hidden layer's output is acquired and saved. On the time axis, the backward layer is computed in reverse. Every time, the backward concealed layer's final result is retrieved and maintained. In the end, the forward and backward layer output values may be combined at each time to get the final output, which can be represented as [25]

$$h_t^F = f\left(w_1 \tilde{x}_t + w_2 h_{t-1}\right), \quad (12)$$

Algorithm 1 The Proposed Signal Detection for OTFS-NOMA Scheme

The inputs: $N, M, M_{mode}, M_{bit}, N_{fr}, SNR, \alpha_{far}, \alpha_{near}$

for *iesn = 1 : length(SNR)* ***do***
  for *ifram = 1 :* N_{fr} ***do***

- Generate random data information bit and convert information bit into symbols
- Modulate $info_{sym}$ with 4-QAM and calculate $x_i[k, l]$
- Compute the signal of the NOMA users using $\alpha_{far}, \alpha_{near}$ in (1)
- OTFS modulation:

$$s_i(t) = \sum_{n=0}^{N-1} \sum_{m=0}^{M-1} \sqrt{\xi_i \alpha_i} X_i[n, m] g_{tx}(t - nT) e^{j2\pi m\Delta f(t-nT)}$$

- Generate Rayleigh channel according to taps, delay-taps, Doppler-taps and chan-coef
- OTFS demodulation:

$$r_i(t) = \iint h_i(\tau, v) s_i(t - \tau) e^{j2\pi v(t-\tau)} d\tau dv + w_i(t)$$

- Decomposition of real part and imaginary part of the output signal $r^{(I)}$ and $r^{(Q)}$
- Decomposition of calculated QAM symbols $x_i^{(I)}[k, l]$ and $x_i^{(Q)}[k, l]$

  end *for ifram*
end *for iesn*

- Training with deep learning model

Parameters: input $r(2, 1)$*, output* $x(2, 1)$
 # BiLSTM Classifier

  for *each sample in r(t)* ***do***

    Calculate Forward Pass of r(t)
    Calculate Backward Pass of r(t)
    Calculate y(t)

  end *for each sample in r(t)*

- Calculate loss function

$$L(\text{ loss }) = \frac{1}{N_B} \sum_{i=1}^{N_B} \left[\hat{x}(i) - x(i)\right]^2$$

- Obtain OTFS-NOMA output symbols $y(t)$ with test model
- Compute $SER = xor(y(t), info_{sym})$

The outputs: L, SER

$$h_t^B = f\left(w_3 \tilde{x}_t + w_4 h_{t+1}\right), \tag{13}$$

$$x_t^{Bi} = o_t \left(w_5 h_t^F + w_6 h_t^B\right) \tanh\left(C_t\right), \tag{14}$$

where h_t^F, h_t^B and x_t^{Bi} indicate the production of the forward and backward computation at time t, and the final output of the BiLSTM, respectively. Here, in LSTM, C_t stands for the cell state and o_t shows the forgetting factor. $\tilde{x}$ defined present LSTM's input while h_{t-1} and h_{t+1} are the last LSTM's output and the output of LSTM in the reverse directions, respectively. $w_1, w_2, w_3, w_4, w_5, w_6$ are matching weights for the variables. Here, $\tanh(\cdot)$ indicates the hyperbolic tangent activation function. Because BiLSTM is capable of learning by analyzing past and future data, it is possible to learn a better intrinsic correlation of the input series signal. Therefore, it holds the potential to improve the signal detection performance in OTFS-NOMA.

BiLSTM is a structure that is composed of multiple LSTM cells. It is a form of recurrent neural network (RNN) architecture which extends the traditional LSTM by processing input sequences. Figure 3 also depicts the basic architecture of the LSTM cell. In order to obtain the f_t for the cell state update, the LSTM forget gate first decides which data to discard. After then, the input gate renovates the crucial data i_t and decides which information is beneficially retained for the candidate cell state $\bar{C}_t$. The status of the cell can be defined as [22]

$$C_t = f_t C_{t-1} + i_t \bar{C}_t. \tag{15}$$

Ultimately, the output gate computes the forgetting factor o_t based on h_{t-1} and the input data $\tilde{x}$. It derives the final output h_t from o_t and the cell state C_t

$$o_t = \sigma\left(w_o\left(h_{t-1}, \tilde{x}_t\right) + b_o\right), \tag{16}$$

$$h_t = o_t \tanh\left(C_t\right), \tag{17}$$

where b_o exhibits o_t's bias and w_o expresses o_t's weight.

The BiLSTM layer has a good strength to obtain time series data interaction. Utilizing the gate structure enables the system to not just retain related data while disregarding unrelated information, but also allows for the extraction of properties from both the forward and reverse aspects. Consequently, when dealing with the signal identification in interfering subsequent data, BiLSTM enhances the memory of the neural network and facilitates the extraction of valuable information by considering sequentially conveyed symbols from prior to the future [25].

The training procedure has a serious impact on the performance of a neural network. To begin, the loss function should be appropriately produced in order to supply an accurate estimate. The training approach tries to decrease the difference between the transmitted data and the deep learning model's signal detection output. The half mean squared error loss (HMSE) function can be defined as [24],

$$L(\text{ loss }) = \frac{1}{N_B} \sum_{i=1}^{N_B} \left[\hat{x}(i) - x(i)\right]^2, \tag{18}$$

where N_B is the batch size. Furthermore, hyperparameters relating to network topology and training will have an impact on neural network capabilities. The learning rate influences the DL network's convergence rate and results.

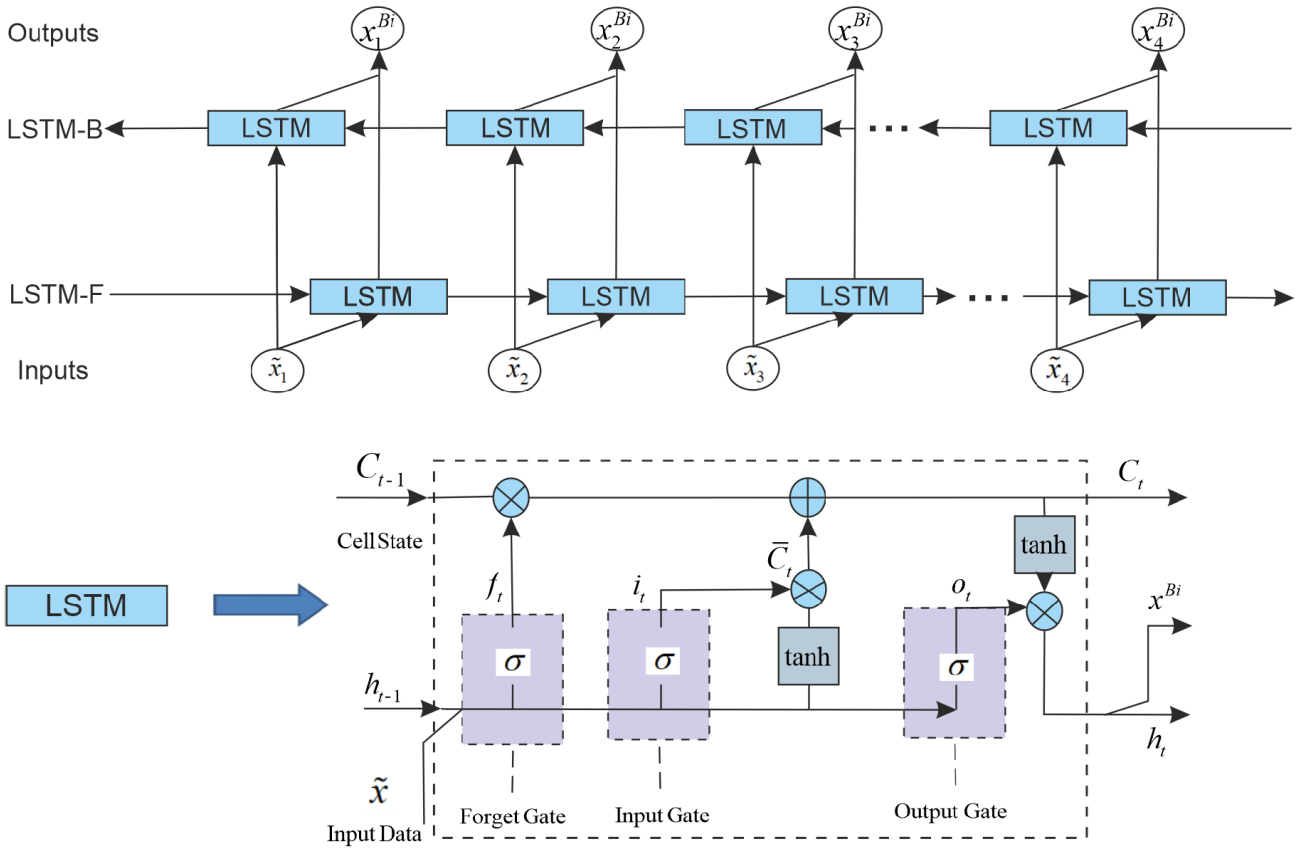

FIGURE 3. BiLSTM architecture.

V. NUMERICAL RESULTS

This section presents the SER achievement of the power domain downlink OTFS-NOMA with the proposed signal detection approaches, namely the MP algorithm and BiLSTM using 4-QAM modulation in a Rayleigh distribution. The PA coefficient for the far user is considered to be 0.85 and 0.15 for the near user. The program is developed in the Matlab environment on a workstation equipped with an Intel(R) Core^{TM} i7-10700K central processing unit (CPU) running at 3.80 GHz, 64 GB of RAM, and an NVIDIA GeForce RTX 2060 graphics processing unit (GPU).

TABLE 2. Simulation parameters for OTFS-NOMA.

Parameter	Value
Number of paths (P_i)	4
Modulation	4-QAM
Carrier frequency (f_c)	4 GHz
Maximum speed (Kmph)	506.25 Kmph
Subcarrier Spacing (Δ_f)	15 kHz
Delay-Doppler Grid Size	$M = 8, N = 8$
Delay tap index	[0 1 2 3]
Delay (μs)	[0 8.33 16.66 24.99]
Doppler tap index	[0 0 1 1]
Doppler (kHz)	[0 0 1.875 1.875]
Fading	Rayleigh
Noise	AWGN

TABLE 3. Training parameters for OTFS-NOMA.

Parameter	Value
Mini batch size	1024
Learning rate	0.001
Learning optimizer	SGD, Adam, RMSprop
Maximum Epoch	16000
Sequence Length	2
Training Sample	1248
Loss Function	HMSE
Gradient Threshold	1

With the aid of the references, [25] and [35], the computational complexity of the BiLSTM can be expressed as $O((NM)^2)$ where (NM) is the OTFS frame size for the network input.

Table 2 shows a list of the simulation parameters. Here, $M = 8, N = 8$ represents the DD grid size, and the number of propagation paths is assumed to be $P_i = 4$. $f_D = \upsilon(f_c)/c$ characterizes the carrier frequency offset. In this formula, c denotes the light speed, υ represents the movement speed between the transceivers, and f_c defines the carrier frequency. The Doppler shift for every path, v_i, is expressed as $v_{max} \cos(\theta_i)$, where θ_i is uniformly distributed over the range of $(-\pi, \pi)$, and $v_{max} = 1.875$ kHz represents the maximum Doppler shift associated with a maximum speed of 506.25 kmph.

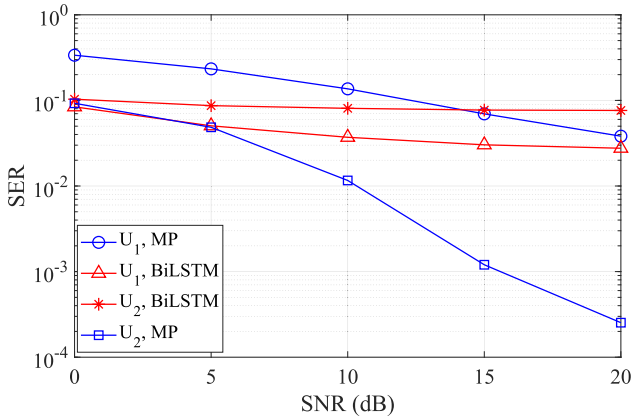

FIGURE 4. SER of BiLSTM for SGD optimizer.

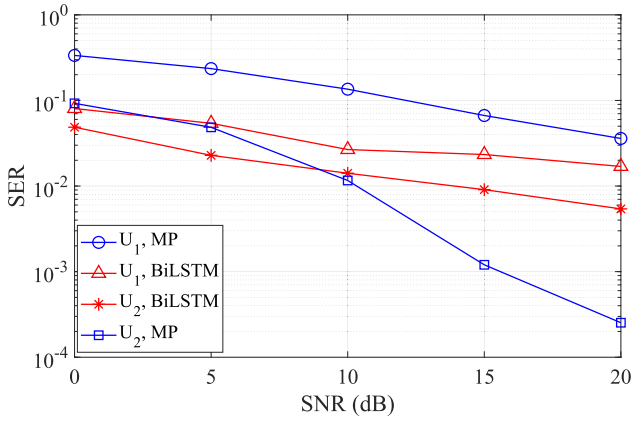

FIGURE 5. SER of BiLSTM for Adam optimizer.

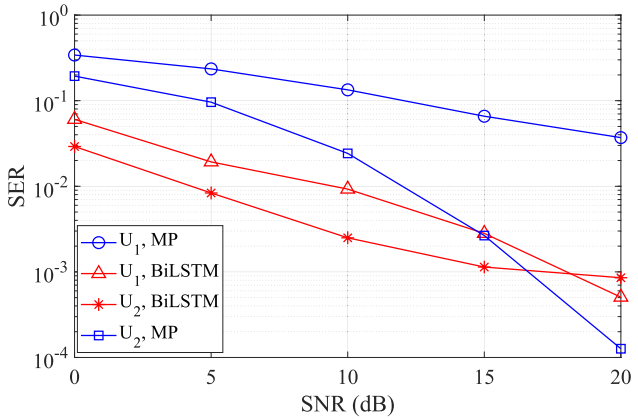

FIGURE 6. SER of BiLSTM for RMSprop optimizer.

The training parameters are shown in Table 3. The effectiveness of neural networks is impacted by the hyperparameters linked to both their structure and training process. The convergence rate and the output of the DL network are modified by the learning rate. The starting learning rate in our training is set at 0.001, the minimum and maximum batch sizes are 1024 and 16000, the sequence length is 2, and the training sample is 1248. The input parameters of

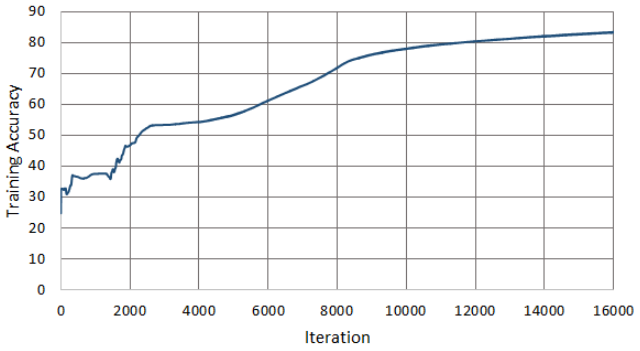

FIGURE 7. The training accuracy for the SGD optimizer.

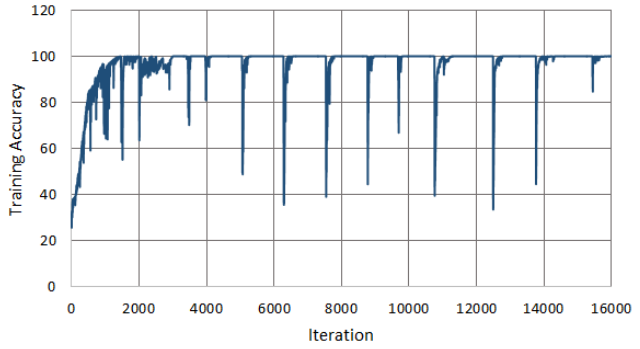

FIGURE 8. The training accuracy for the Adam optimizer.

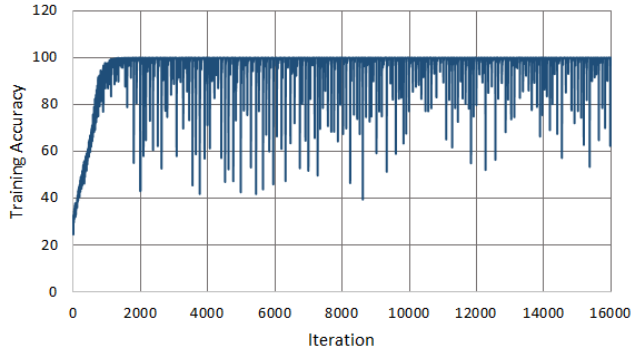

FIGURE 9. The training accuracy for the RMSprop optimizer.

the dataset are taken as symbols in the receiver section, and the symbol at the input of the transmitter is taken as the output parameter. The BiLSTM trains the data over four classes (0, 1, 2, 3) for modulation type 4-QAM. These class values represent the signals 00, 01, 10, and 11, respectively. The class values indicate the decimal value of the message signals transmitted in end-to-end communication systems. The LSTM layer consists of 600 hidden cells. The training process utilizes 80% of the dataset, with the remaining 20% allocated for testing the trained network.

We assessed the efficacy of three widely used optimizers for training: SGD, Adam, and RMSprop optimizers. Figure 4 illustrates the SER performances of near and far users for the SGD optimizer. While the BiLSTM method yields better

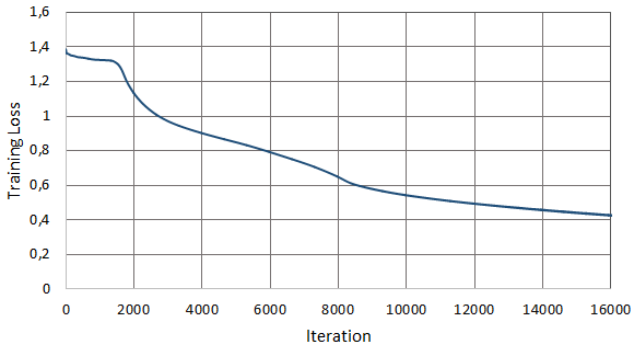

FIGURE 10. The training loss for the SGD optimizer.

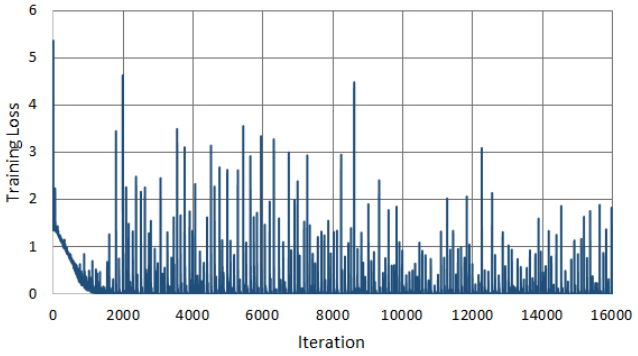

FIGURE 11. The training loss for the RMSprop optimizer.

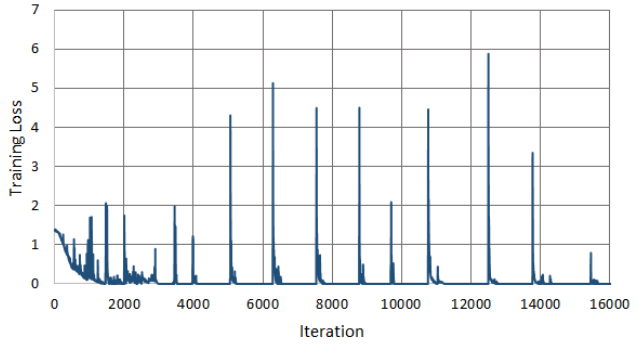

FIGURE 12. The training loss for the Adam optimizer.

results than the MP method for the near user, the performance of MP is superior when considering the far user. This situation may be attributed to the slow learning of SGD.

In Figure 5, upon evaluating the SER performance with respect to signal-to-noise ratio (SNR), better outcomes are noted with the Adam optimizer in comparison to the SGD optimizer. Figure 6 provides the SER performance varying with SNR for the RMSprop optimizer. As seen in the figure, RMSprop demonstrates significantly better results compared to the other two optimizers.

Figures 7-9 illustrate the training accuracy for the SGD, Adam, and RMSprop, respectively. In the training stage, SGD, Adam, and RMSprop have led to training accuracies of 83.72%, 99.9%, and 99.9%, respectively. To facilitate the classification of sequence data through the training of a deep neural network, an LSTM network was employed. An LSTM network lets users enter sequence data into a network and make guesses based on the separate time steps of the data array. The generation of the distinct predictions for every time step of the sequence data is utilized by a sequence-to-sequence LSTM network. In addition, at each time, a bidirectional LSTM layer learns using the entire sequence. This makes it highly effective in understanding and predicting patterns in sequential data. During the training of the deep model, the low-level loss function performed at high accuracy levels. This training state overcomes the limitations of the sequence-to-sequence prediction of the SER.

Figures 10-11 demonstrate the training loss for the SGD, Adam, and RMSprop, respectively. The loss of the suggested neural network fails to converge efficiently when employing the SGD optimizer during the training phase. In the context of convergence, the Adam optimizer demonstrated superior performance compared to the SGD optimizer, while the RMSprop optimizer surpassed both of them.

VI. CONCLUSION

This study examines the SER performance comparison between the MP detector and a BiLSTM-based neural network designed for signal detection in OTFS-NOMA communication. The numerical results demonstrate that the SER performance of BiLSTM is better for the RMSprop optimizer than the MP signal detection method in OTFS-NOMA. The simulation results illustrate that the system's performance is notably influenced by the PA coefficient, delays, and Doppler effects.

While our investigation primarily focused on assessing the SER performance of OTFS-modulated NOMA systems in a high-mobility environment with two destination users, it is feasible to expand the analysis to yield more generalized insights applicable to emerging 6G mobile network technologies. This includes the integration of reconfigurable intelligent surfaces (RIS), unmanned aerial vehicles (UAVs) [31], integrated sensing and communications (ISAC) and non-terrestrial networks. Incorporating the above-mentioned technologies into NOMA systems over OTFS holds promise for advancing the scope of our future research. Additionally, exploring cognitive radio architectures [32], [33] presents an alternative scenario. Investigating secondary user signal detection algorithms aimed at improving spectral efficiency in high-speed mobile environments is another subject for our research. Furthermore, our upcoming work plans encompass exploring channel estimation strategies, reliability, and physical layer security investigation [34] specifically tailored for OTFS-modulated NOMA systems.

ACKNOWLEDGMENT

The authors would like to thank Assoc. Prof. Omer Kasim from Kutahya Dumlupinar University, for supplying the datasets treated here and for the insightful discussion,

constructive criticisms, valuable advice, and guidance on DL-based signal detection.

ACRONYMS

4G	Fourth Generation.
5G	Fifth Generation.
6G	Sixth Generation.
Adam	Adaptive Momentum.
AWGN	Additive White Gaussian Noise.
BER	Bit Error Rate.
BiLSTM	Bidirectional Long Short-Term Memory.
CIR	Channel Impulse Response.
CNN	Convolutional Neural Network.
CPU	Central Processing Unit.
DD	Delay-Doppler.
DLD	Delay-based Detector.
DNN	Deep Neural Network .
DSL	Digital Subscriber Line.
FC-DNN	Fully Connected Deep Neural Network.
GPU	Graphics Processing Unit.
ICI	Intercarrier Interference.
IRS	Integration of Intelligent Surfaces.
ISAC	Integrated Sensing and Communications.
ISFFT	Inverse Symplectic Fast Fourier Transform .
LMMSE	Linear Minimum Mean Squared Error.
LSTM	Long Short-Term Memory.
LSTM-B	Long Short-Term Memory - Backward.
LSTM-F	Long Short-Term Memory - Forward.
LTE	Long-Term Evaluation.
MP	Message Passing.
MUI	Multi-User Interference.
NOMA	Non-Orthogonal Multiple Access.
OFDM	Orthogonal Frequency Division Multiplexing.
OMA	Orthogonal Multiple Access.
OTFS	Orthogonal Time Frequency Space.
PA	Power Allocation .
QAM	Quadrature Amplitude Modulation.
ResCNN	Residual Convolutional Neural Network.
RMSprop	Root Mean Squared Propagation.
RNN	Recurrent Neural Network.
SC	Superposition Coding .
SE	Spectral Efficiency.
SER	Symbol Error Rate.
SFFT	Symplectic Fast Fourier Transform.
SGD	Stochastic Gradient Descent.
SIC	Successive Interference Cancellation.
SNR	Signal-to-Noise Ratio.
TF	Time-Frequency.
UAV	Unmanned Aerial Vehicles.
UWA	Underwater Acoustic.
ZF	Zero Forcing.

REFERENCES

[1] H. Tataria, M. Shafi, A. F. Molisch, M. Dohler, H. Sjöland, and F. Tufvesson, "6G wireless systems: Vision, requirements, challenges, insights, and opportunities," *Proc. IEEE*, vol. 109, no. 7, pp. 1166–1199, Jul. 2021.

[2] Z. Wei, W. Yuan, S. Li, J. Yuan, G. Bharatula, R. Hadani, and L. Hanzo, "Orthogonal time-frequency space modulation: A promising next-generation waveform," *IEEE Wireless Commun.*, vol. 28, no. 4, pp. 136–144, Aug. 2021.

[3] R. Hadani, S. Rakib, M. Tsatsanis, A. Monk, A. J. Goldsmith, A. F. Molisch, and R. Calderbank, "Orthogonal time frequency space modulation," in *Proc. IEEE Wireless Commun. Netw. Conf. (WCNC)*, Mar. 2017, pp. 1–6.

[4] S. McWade, M. F. Flanagan, and A. Farhang, "Low-complexity equalization and detection for OTFS-NOMA," in *Proc. IEEE Int. Conf. Commun. Workshops (ICC Workshops)*, May 2023, pp. 530–535.

[5] P. Raviteja, K. T. Phan, Y. Hong, and E. Viterbo, "Interference cancellation and iterative detection for orthogonal time frequency space modulation," *IEEE Trans. Wireless Commun.*, vol. 17, no. 10, pp. 6501–6515, Oct. 2018.

[6] Z. Kang, H. Zhao, and H. Wang, "An efficient two-dimension OTFS-NOMA scheme based on heterogenous mobility users grouping," in *Proc. IEEE 21st Int. Conf. Commun. Technol. (ICCT)*, Oct. 2021, pp. 726–730.

[7] L. Xiao, S. Li, Y. Qian, D. Chen, and T. Jiang, "An overview of OTFS for Internet of Things: Concepts, benefits, and challenges," *IEEE Internet Things J.*, vol. 9, no. 10, pp. 7596–7618, May 2022.

[8] Z. Wang, Z. Liu, Z. Sun, and X. Ning, "BER performance analysis of OTFS systems with power allocation," *China Commun.*, vol. 20, no. 1, pp. 24–35, Jan. 2023, doi: 10.23919/JCC.2023.01.003.

[9] L. Dai, B. Wang, Z. Ding, Z. Wang, S. Chen, and L. Hanzo, "A survey of non-orthogonal multiple access for 5G," *IEEE Commun. Surveys Tuts.*, vol. 20, no. 3, pp. 2294–2323, 3rd Quart., 2018.

[10] I. Umakoglu, M. Namdar, A. Basgumus, F. Kara, H. Kaya, and H. Yanikomeroglu, "BER performance comparison of AF and DF assisted relay selection schemes in cooperative NOMA systems," in *Proc. IEEE Int. Black Sea Conf. Commun. Netw. (BlackSeaCom)*, Bucharest, Romania, May 2021, pp. 1–6.

[11] G. D. Surabhi, R. Mary Augustine, and A. Chockalingam, "Multiple access in the delay-Doppler domain using OTFS modulation," 2019, *arXiv:1902.03415*.

[12] Z. Ding, R. Schober, P. Fan, and H. Vincent Poor, "OTFS-NOMA: An efficient approach for exploiting heterogenous user mobility profiles," *IEEE Trans. Commun.*, vol. 67, no. 11, pp. 7950–7965, Nov. 2019.

[13] K. Deka, A. Thomas, and S. Sharma, "OTFS-SCMA: A code-domain NOMA approach for orthogonal time frequency space modulation," *IEEE Trans. Commun.*, vol. 69, no. 8, pp. 5043–5058, Aug. 2021.

[14] A. Chatterjee, V. Rangamgari, S. Tiwari, and S. S. Das, "Nonorthogonal multiple access with orthogonal time–frequency space signal transmission," *IEEE Syst. J.*, vol. 15, no. 1, pp. 383–394, Mar. 2021.

[15] P. Raviteja, E. Viterbo, and Y. Hong, "OTFS performance on static multipath channels," *IEEE Wireless Commun. Lett.*, vol. 8, no. 3, pp. 745–748, Jun. 2019.

[16] S. Tiwari, S. S. Das, and V. Rangamgari, "Low complexity LMMSE receiver for OTFS," *IEEE Commun. Lett.*, vol. 23, no. 12, pp. 2205–2209, Dec. 2019.

[17] K. R. Murali and A. Chockalingam, "On OTFS modulation for high-Doppler fading channels," in *Proc. Inf. Theory Appl. Workshop (ITA)*, San Diego, CA, USA, Feb. 2018, pp. 1–10.

[18] K. David, J. Elmirghani, H. Haas, and X. -H. You, "Defining 6G: Challenges and opportunities," *IEEE Veh. Technol. Mag.*, vol. 14, no. 3, pp. 14–16, Sep. 2019.

[19] N. Kato, B. Mao, F. Tang, Y. Kawamoto, and J. Liu, "Ten challenges in advancing machine learning technologies toward 6G," *IEEE Wireless Commun.*, vol. 27, no. 3, pp. 96–103, Jun. 2020.

[20] B. Ozpoyraz, A. T. Dogukan, Y. Gevez, U. Altun, and E. Basar, "Deep learning-aided 6G wireless networks: A comprehensive survey of revolutionary PHY architectures," *IEEE Open J. Commun. Soc.*, vol. 3, pp. 1749–1809, 2022.

[21] H. Ye, G. Y. Li, and B.-H. Juang, "Power of deep learning for channel estimation and signal detection in OFDM systems," *IEEE Wireless Commun. Lett.*, vol. 7, no. 1, pp. 114–117, Feb. 2018.

[22] J. Li, T. Xin, B. He, and W. Li, "IQ symbols processing schemes with LSTMs in OFDM system," *IEEE Access*, vol. 10, pp. 70737–70745, 2022.

[23] S. Wang, R. Yao, T. A. Tsiftsis, N. I. Miridakis, and N. Qi, "Signal detection in uplink time-varying OFDM systems using RNN with bidirectional LSTM," *IEEE Wireless Commun. Lett.*, vol. 9, no. 11, pp. 1947–1951, Nov. 2020.

[24] A. Emir, F. Kara, H. Kaya, and X. Li, "Deep learning-based flexible joint channel estimation and signal detection of multi-user OFDM-NOMA," *Phys. Commun.*, vol. 48, Oct. 2021, Art. no. 101443.
[25] Y. Zhang, S. Zhang, B. Wang, Y. Liu, W. Bai, and X. Shen, "Deep learning-based signal detection for underwater acoustic OTFS communication," *J. Mar. Sci. Eng.*, vol. 10, no. 12, p. 1920, Dec. 2022.
[26] D. Chen, G. Xiong, B. Huang, and L. Wang, "Modulation signal recognition based on feature fusion and residual CNN in fractal noise background," in *Proc. IEEE 6th Int. Conf. Signal Image Process. (ICSIP)*, Nanjing, China, Oct. 2021, pp. 687–691.
[27] E. Xu, G. Xiong, S. Zhang, and H. Zhao, "HRRP target recognition based on the dual-mode Gram angle field features and the multi-level CNN," in *Proc. IEEE 6th Int. Conf. Signal Image Process. (ICSIP)*, Nanjing, China, Oct. 2021, pp. 77–81.
[28] I. Umakoglu, M. Namdar, A. Basgumus, S. Özyurt, and S. Kulaç, "BER performance analysis for NOMA systems with OTFS modulation," in *Proc. 31st Signal Process. Commun. Appl. Conf. (SIU)*, Jul. 2023, pp. 1–4.
[29] I. Umakoğlu, M. Namdar, and A. Başgümüş, "Performance evaluation of OTFS-NOMA scheme for high mobility users," *Sakarya Univ. J. Comput. Inf. Sci.*, vol. 6, no. 3, pp. 253–260, Dec. 2023.
[30] T. Thaj and E. Viterbo, "Low complexity iterative rake detector for orthogonal time frequency space modulation," in *Proc. IEEE Wireless Commun. Netw. Conf. (WCNC)*, Seoul, Korea (South), May 2020, pp. 1–6.
[31] I. Umakoglu, M. Namdar, and A. Basgumus, "UAV-assisted cooperative NOMA system with the nth best relay selection," *Adv. Electr. Comput. Eng.*, vol. 23, no. 3, pp. 39–46, 2023.
[32] F. K. Bardak, M. Namdar, and A. Basgumus, "Ergodic capacity analysis of the relay assisted downlink NOMA systems in cognitive radio networks," *J. Eng. Sci. Des.*, vol. 9, no. 3, pp. 992–1002, 2021.
[33] M. Namdar, A. Guney, F. K. Bardak, and A. Basgumus, "Ergodic capacity estimation with artificial neural networks in NOMA-based cognitive radio systems," *Arabian J. Sci. Eng.*, vol. 49, no. 5, pp. 6459–6468, May 2024.
[34] A. Basgumus, M. S. Ardic, and M. Namdar, "Capacity analysis of the secondary users in spectrum sharing model over Nakagami-*m* and log-normal fading channels," *J. Fac. Eng. Archit. Gazi Univ.*, vol. 38, no. 4, pp. 2205–2212, 2023.
[35] K. He and J. Sun, "Convolutional neural networks at constrained time cost," in *Proc. IEEE Conf. Comput. Vis. Pattern Recognit. (CVPR)*, Boston, MA, USA, Jun. 2015, pp. 5353–5360.

INCI UMAKOGLU (Member, IEEE) received the B.Sc. degree from the Department of Electronics and Communications Engineering, Kocaeli University, Kocaeli, Türkiye, in 2014, and the M.Sc. and Ph.D. degrees from the Department of Electrical and Electronics Engineering, Kutahya Dumlupinar University, Kütahya, Türkiye, in 2017 and 2024, respectively. Her current research interests include NOMA, relay networks, and their applications to wireless communications.

MUSTAFA NAMDAR (Member, IEEE) received the B.Sc. and Ph.D. degrees from the Department of Electronics and Communications Engineering, Yildiz Technical University, Istanbul, Türkiye. From 2000 to 2011, he was at Turkcell, Istanbul, Türkiye, where he participated in several wireless communications projects. He joined with the Department of Electrical and Electronics Engineering, Kutahya Dumlupinar University, Kütahya, Türkiye, in 2015. He is a member of the Information and Communications Research Group (ICRG), Istanbul Technical University (ITU), and also a partner of the 6G Platform. His current research interests include cognitive radio networks, cooperative communications, relay networks, interference alignment, NOMA, and RIS. He has also served as a TPC member for the several IEEE international conferences. He received the Outstanding Reviewer Award of the Elsevier-AEU Journal, in 2017, and the IEEE SIU Conference, in 2023. He served as a reviewer for several IEEE journals.

ARIF BASGUMUS (Member, IEEE) received the B.Sc. and Ph.D. degrees from the Department of Electronics Engineering, Bursa Uludag University, Bursa, Türkiye. He is currently working as an Associate Professor with the Department of Electrical and Electronics Engineering, Bursa Uludag University. He is a member of the Information and Communications Research Group (ICRG), Istanbul Technical University (ITU), and also a partner of the 6G Platform. His current research interests include cognitive radio networks, cooperative communications, relay networks, interference alignment, NOMA, RIS, and optimization algorithms. He served as a Reviewer for several journals including IEEE, IET, Elsevier Journals, and IEEE International Conferences.